

EFFECTIVE THERMAL CONDUCTIVITIES OF UNIT-LATTICE STRUCTURES FOR MULTI-FUNCTIONAL COMPONENTS

D. Cook^{*}, S. Newbauer^{*}, D. Pettis^{*}, B. Knier[†] and S. Kumpaty, Ph.D., P.E.[§]

^{*}Applied-Technology Center, Rapid-Prototyping Research, Milwaukee School of Engineering, Milwaukee, WI 53202

[†]MS Mechanical Engineering Student, UW Madison, Madison, WI 53202

[§]Department of Mechanical Engineering, MS Engineering Program Director, Milwaukee School of Engineering, Milwaukee, WI 53202

Abstract

Approaching the goal of automatically generating optimized multi-functional components, previously-identified unit-lattice structures are being characterized for their geometry-dependent, effective, thermal conductivities. This knowledge base will allow for the definition of low-mass, load-bearing, thermal-management structures. One application is a wearable power source for a custom, portable, active orthosis. The function of this structure is to bear mechanical load while dissipating heat from the source, without burning the wearer. Additive manufacturing affords the capability of fabricating the resultant complex structures. Current research efforts are using finite-element analysis and physical testing to validate the characteristic models, and determining the scale dependence of internal-convective-flow development. Future work will include composites.

Nomenclature

Initialisms:

AM:	Additive manufacturing
CCEFP:	Center for Compact and Efficient Fluid Power
CFD:	Computational fluid dynamics
ERC:	Engineering Research Center
FEA:	Finite-element analysis
MSE:	Milwaukee School of Engineering
NSF:	National Science Foundation
TMS:	Thermal-management structure

Variables:

α :	Thermal diffusivity (m^2/s)
β :	Coefficient of thermal expansion (T^{-1})
Δ :	Delta, "change in" (ex.: ΔT is change in temperature)
η :	Efficiency
ρ :	Density (Kg/m^3)
\emptyset :	Diameter (m)
A:	Cross-sectional area (m^2)
F_b :	Buoyancy force (N/m^3)

g:	Gravitational constant ($9.81m/s^2$)
Gr:	Grashof number – Ratio of the buoyancy forces to viscous forces in a fluid
h:	Thermal convection coefficient ($W/m^2 * K$)
k:	Thermal conductivity ($W/m * K$)
$k_{\text{effective}}$:	Effective thermal conductivity ($W/m * K$)
L:	Length (m)
Pr:	Prandtl number – Ratio of kinematic viscosity to thermal diffusivity
q:	Heat rate (W)
q'' :	Heat-rate flux (W/m^2)
Ra:	Rayleigh number – Used to determine if natural convection will occur
r_{cr} :	Critical radius of insulation (m)
R_t :	Thermal resistance (W/K)
T:	Temperature (K)

Introduction

A. Purpose:

All real systems have a degree of inefficiency, the majority of which is converted to heat. Internal-combustion engines, for example, average only 25% efficiency. For a 74.6kW (100Hp) engine, that is roughly 56kW of wasted energy, of which at least half is waste heat. That is 50MJ of wasted energy for a half-hour drive (maintaining average power)!

The National Science Foundation's (NSF) Engineering Research Center (ERC), titled the Center for Compact and Efficient Fluid Power (CCEFP), for example, is working to improve system efficiencies of fluid-power systems at all levels, to increase the current average of 40%. This waste heat is not only an immediate loss of input power; it also reduces the viscosity of the oil, reducing the efficiency at which the system can use the power that it does receive. Cooling the oil from 90°C to 80°C, using components with integrated passive thermal management, can improve system efficiency by 20% with minimal increase in mass [Herzog and Neveu, 2011]. Generally, maintaining an operating temperature close to room temperature (at which components are designed by default) will minimize leakage and binding, thereby maximizing efficiency.

Waste heat can also be converted to useful energy that can be fed back into the system, further improving system efficiency. For the above engine example, even at one percent (1%) conversion efficiency, thermoelectric generators could recover more than 280W to power electrical systems [Schneider et al., 2007]; and, efficiencies of 15-20% are anticipated using new materials [Canter, 2011].

Finally, efforts to develop powered personal devices are hindered by the high temperatures generated, that can cause burning, pain or general discomfort. Proper thermal management can mitigate these issues.

The purpose of the research discussed herein is to contribute to a design paradigm, around the freedom afforded by additive manufacturing (AM), for multi-functional components and structures that: effectively manage waste heat, minimizing the detriment to the system (while

also minimizing mass and bearing mechanical loads); improve safety; and, optimize the integration of devices for waste-heat recovery.

B. Background:

Considerable research has been conducted to characterize the thermal properties of cellular and lattice materials with the goal of establishing their benefits as thermal-management and multi-functional materials. Conventional heat sinks are not multi-functional, and generally limited in design by fabrication constraints. Predominantly, the most recent research involves foams, having generally isotropic properties, and homogeneous lattice structures, that do not conform to the application [Wadley, 2002].

Metal foams are increasingly being used, since they can bear moderate loads in multiple directions, and are commercially available. This research takes this trend further to include anisotropic performances of devices for structural and thermal loads (as well as pressure-wave attenuation), and includes component integration, i.e. one component serving the functions of multiple conventional modular ones, making that one a true multi-functional component.

Additionally, this prior research focused on forced-convective fluid flow through the material or structure ([Kim et al., 2004], [Seepersad et al., 2006], [Straatman et al., 2006]). Contrary to the goal of developing multi-functional components that improve system efficiency, including mechanisms to provide this forced convection will detract from the efficiency gains.

The scope of this research is in defining component geometries that provide greater heat efflux and, for personal applications, safe contact temperatures, while also contributing structurally. A portable, powered, ankle-foot orthosis is being developed within the CCEFP, designated as Test Bed 6 ([Human Assist Devices], [Shorter et al.]), for which the power source currently being developed is a small internal-combustion engine ([Project 2B.2], [Tian et al., 2010]). Certainly, there are concerns regarding the safety and noise of this device. The goal is to use the structure to protect the wearer from high temperatures, and provide optimal heat transfer for various components of the system. Future work will include vibration and noise attenuation, as well as load bearing.

For such human-scale components and systems, radial diffusion can be used to achieve these thermal-management goals, even past the critical radius of insulation ([Davis, 2007], [Kulkarni, 2004]):

$$r_{cr} = k/h \quad (1)$$

With sustainability concerns being brought to the forefront, such thermal-management structures can also be optimized to provide the greatest thermal gradient for waste-energy recovery, limited by the Carnot efficiency:

$$\eta = 1 - T_{cold}/T_{hot} \quad (2)$$

Indeed, for mobile systems that require low drag, designing the thermal management of components using stagnant internal fluids and external convection will safeguard the design

against the failure of the internal-forced-convection supply and blockage of mass influx for through-flow convection. Modeling in this way is also greatly simplified. This reference design may then also be used to initiate system optimizations that include such internal fluid flow.

Approach

A. *Unit-Lattice Characterization:*

Several unit-lattice structures had been previously identified for their applicability in generating structurally-optimized components ([Cook and Gervasi, 2011], [Cook et al., 2010]). Toward the goal of generating multi-functional components, three¹ of these structures were characterized for their effective thermal conductivities as well. A unit cell is comprised of eight unit-lattice structures at the vertices of the hexahedral volume (Figure 1).



Figure 1: (Left) unit lattice and (Right) unit cell of the Cube structure type.

A thermal-resistance model had been developed to characterize the thermal properties of carbon foam [Yu et al. 2006]; and, a similar model was developed for the Cube unit cell [Appendix A]. Considering the complexity of the remaining structures, however, another means was required. The conductivity was, therefore, approximated using a rate equation known as Fourier's law [Incropera & Dewitt, 1985]. Assuming that the temperature gradient across the unit cell is uni-directional (one-dimensional), the rate equation is expressed as:

$$q''_x = -k_{effective} dT/dx \quad (3)$$

Where q''_x is the heat flux in the x direction per unit area; $k_{effective}$ is the effective (bulk) thermal conductivity of the cell; and, dT/dx is the temperature gradient across the cell, in the x direction. Approximating the temperature gradient as $\Delta T/\Delta x$, and integrating both sides of the equation with respect to the cross-sectional area, A, Equation 3 becomes:

$$\int q''_x dA = -k_{effective} A \Delta T/\Delta x \quad (4)$$

The negative sign indicates that heat transfer is in the direction of decreasing temperature.

COMSOL® provides the ability to calculate the heat flux using surface integration. Two opposing sides of the cube, in the direction of the desired thermal gradient, were set to a specific temperature differential; and, the other surfaces were considered insulated. The only unknown remaining is the effective thermal conductivity of the material. Initially, the fluid inside the structures is considered to be stagnant, so the effects of convection are neglected. Effectively, the fluid is treated as an insulating solid, thereby creating a composite structure. Certainly, solid

¹ Only three of the five structures were analyzed due to time and budget constraints.

insulators could be used as well, but few approach the low conductivity, mass and cost of air. The first analyses used the following parameters:

- Solid Material: Aluminum ($k = 160 \text{ W/ m}^*\text{K}$)
- Fluid Material: Air (k varies with temperature, approximately $= 0.025 \text{ W/ m}^*\text{K}$)
- Cell Length (ΔX): 0.0254 m (1 in)
- Cell Surface Area (A): $6.45\text{E-}04 \text{ m}^2$ (1 in²)
- Temp Gradient (ΔT) : 100K

The strut diameters, \emptyset , tested were $0.2L$, $0.5L$ and $0.8L$, where L is the edge length of the equilateral cubic cell. With three different directions having three set diameters, 27 different combinations are possible; though, only 10 of them are “unique” combinations, assuming that orientation will not affect the outcome, i.e. K_{xx} of a Cube having $\emptyset_x = 0.2L$, $\emptyset_y = 0.5L$ and $\emptyset_z = 0.5L$ will be equal to K_{yy} of a Cube having $\emptyset_x = 0.5L$, $\emptyset_y = 0.2L$ and $\emptyset_z = 0.5L$. The results of the conductivities for various cell sizing were then tabulated in Microsoft Excel® [Appendix C]; and, a regression tool (LINEST) was used to determine the equations relating the three orthogonal conductivities (K_{xx} , K_{yy} and K_{zz}) to the strut sizes (\emptyset_x , \emptyset_y and \emptyset_z) [Appendix E].

Modifications to the Model:

Initially, the fluid and solid on the sides of the unit cell were assigned the same temperature, since the distribution of heat flux was not known a priori; however, it was determined that this imposes an artificial temperature gradient and heat flux [Appendix B]. To remedy this, copper blocks were added fore and aft of the cell [Figure 2]. By placing the boundary conditions on the copper blocks, the heat flux is allowed to “choose its own path,” allowing for a more natural model.

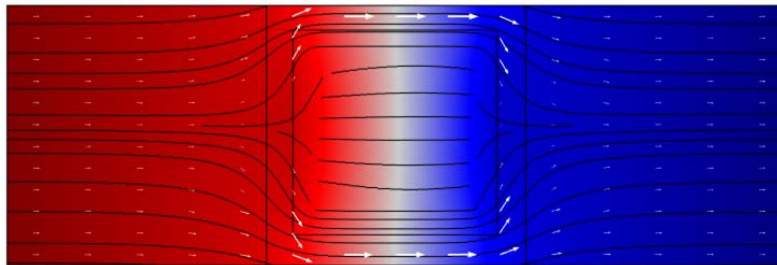


Figure 2: Inclusion of copper blocks in determination of effective thermal conductivity of the unit cell. As shown, the heat flux through the unit cell follows a natural path. For the 3-D structure, this results in non-planar temperatures at the faces of the cell, until the volume fraction of the solid approaches 100%.

Because the conductivity of the copper blocks is known, the conductivity of the unit cell, at steady state, can be calculated using a one-dimensional thermal circuit, analogous to an electrical circuit, consisting of three resistors; two copper blocks, and the fluid-filled cell. The “current” is the total heat flowing through the circuit, with the “voltage” being the temperature differential:

$$\Delta T = q_x R_t \tag{5}$$

Where ΔT is the temperature difference from one node to another, q_x is the total heat flowing through the circuit, and R_t is the overall thermal resistance. Because the model was set up as a series model, the effective resistance follows the relationship of:

$$R_t = R_1 + R_2 + R_3 \quad (6)$$

Where R_1 , R_2 and R_3 are the respective resistors in the circuit. Solving for the conductivity of the fluid-filled unit cell is now just a matter of algebraic manipulation. Thermal resistance can be related to conductivity by:

$$R_n = \Delta X / k_n A \quad (7)$$

COMSOL® uses 400 W/m*K as the conductivity of copper, with the copper block being 25.4 mm x 25.4 mm x 25.4 mm, resulting in a resistance of 0.0984252 K/W for each.

B. Unit-Cell Convection:

Initially, the air inside the structure was considered to be stagnant, so the effects of convection could be ignored; but, if the temperature difference across the cell becomes large enough, the fluid will start to move, driven by buoyancy forces due to a difference in density, generated by the temperature gradient. This is called “free” or “natural” convection. In consideration of these cellular structures, two cases of enclosed natural convection will be discussed.

If the temperature gradient occurs in the direction of the gravitational forces, two possible situations arise. One occurs when the density decreases in the direction of gravity. This will cause an unstable temperature gradient; and, the fluid will circulate. The second situation occurs when the density gradient acts in the opposite direction of gravity. This produces a stable temperature gradient; and, the fluid is stagnant. Alternatively, the temperature gradient may be perpendicular to the gravitational forces (Figure 3), similar to a window.

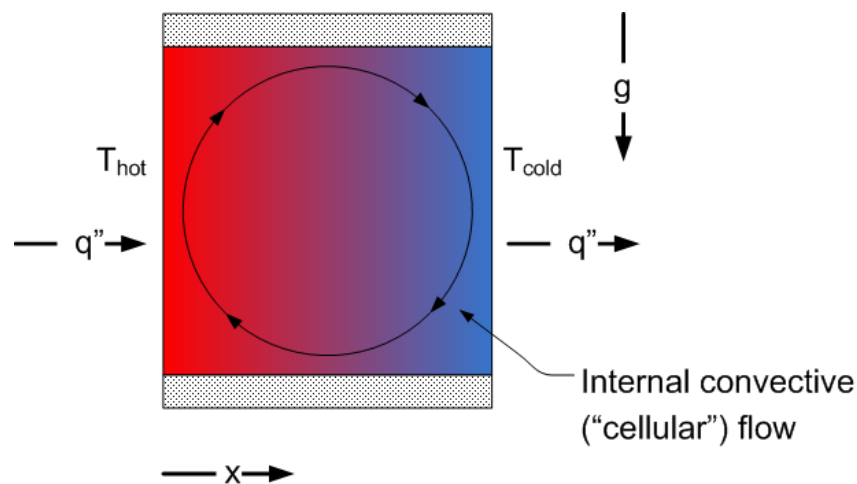


Figure 3: Development of cellular convective flow for a density gradient and one-dimensional heat flux perpendicular to the direction of gravity.

The questions are: “At what scale and temperature gradient will natural convection develop inside individual cubes;” and, “How will this change the effective conductivity?”

When will convection start?

Natural convection occurs when the buoyancy forces in the fluid overcome the viscous forces. This transition can be predicted from the Rayleigh number, Ra, defined as the product of the Grashof, Gr, and Prandtl, Pr, numbers. The Grashof number is the ratio of the buoyancy forces to the viscous forces acting on the fluid [Incropera & Dewitt 1985]. When the Rayleigh number reaches a critical number, natural convection will occur. In the case of natural convection inside a cavity, the critical number is 1708. Therefore, natural convection will occur when:

$$Ra_x = Gr_x Pr = \frac{g\beta(T_1 - T_2)L^3}{\alpha\nu} > 1708 \quad (5)$$

Where L is the characteristic length. Figure 4 shows the necessary characteristic length required for natural convection to occur, in relation to the temperature gradient across the cell.

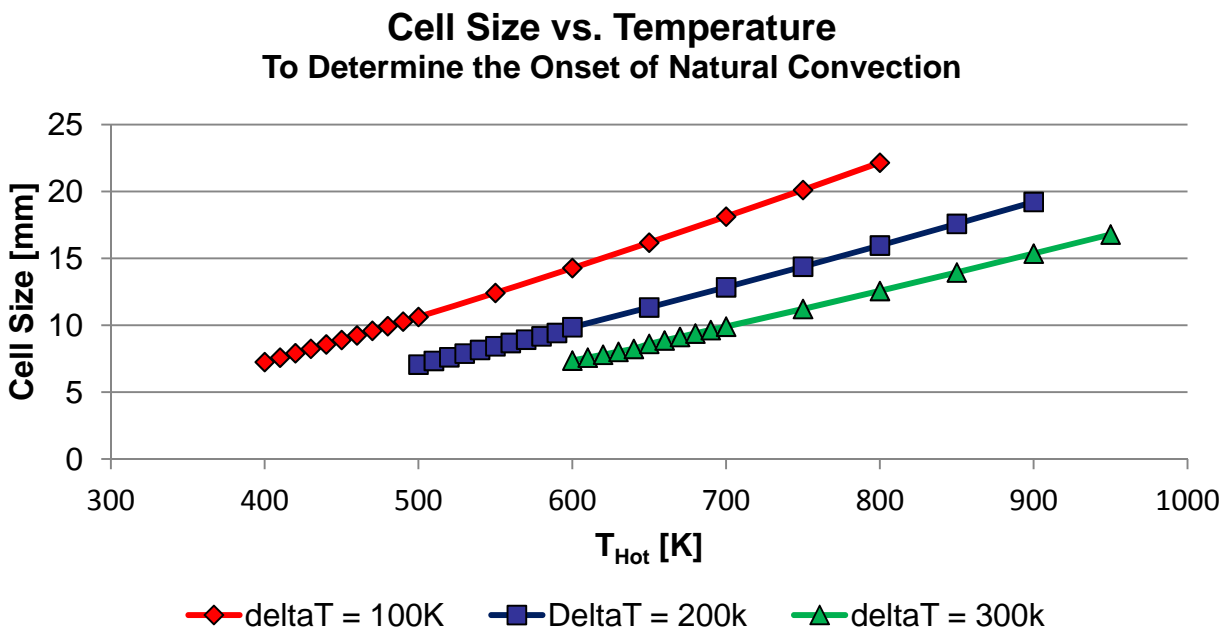


Figure 4: Lower temperature differentials across the unit cells allows for larger cell sizes before the onset of internal natural convection.

How will effective conductivity be affected by convection?

Double-paned windows are used in homes because the air film acts as an insulator; however, if convective currents develop inside a window, the total heat transfer across the window will increase. It was initially expected that similar results would occur with the cubes. To test this, models were set up in COMSOL®. The setup was similar to that of earlier tests, with a unit cell structure and adjacent copper blocks, and temperatures set at the ends of the copper. A local volume force, F_b , was applied to the fluid using the density calculated by the

non-isothermal-flow solver to approximate the buoyancy force created when the fluid heats up and expands:

$$\vec{F}_b = -\rho_{nitf} * \vec{g} \quad (6)$$

Where ρ is the density of the fluid at a given node, and g is the gravitational constant (9.81 m/s²). Again, only cubic volumes were analyzed; limiting the number of analyses to be conducted, and matching the expected cubic nature of the resultant multi-functional structure.

C. Conductivity Optimization:

Initial finite-element analysis (FEA) Steps

In order to design a thermal-management structure (TMS) with a desired temperature drop, the scale of the thermal conductivity must be known. A 2-D axi-symmetric structure was designed within COMSOL®. The cylinder had a hollow inner radius, representing the heat source. The inner and outer radii of the structure were selected; and, a hemi-spherical top was added to enclose the heat source. The model was then divided into subsections, each assigned material properties that closely resembled those of insulators. A temperature was prescribed at the inner radius of the structure; and, natural convection at room temperature was specified at the outer radius of the component. The model was solved for the temperature at the outer surface. The subsections were then redefined with new material properties until a desired temperature drop was achieved. This was a manual iterative optimization, but, will be automated in future work. Once the desired temperature drop was achieved, the scales of the thermal conductivities for each subsection were noted. These were then used in designing the preliminary structure.

Preliminary Structure Design

The bulk thermal conductivity of the unit lattice structures had been determined as well as the target thermal conductivities of the structure design. To design the preliminary structure with the derived unit-cell, geometry-dependent, effective-conductivity relations, the subsections of the structure had to be kept as cubic as possible. Geometric relations determining the distance of each strut from the center of the cylinder and height of each subsection were derived based on the; number of radial components, number of columns, and radii of the structure. A script was written to calculate these values, varying the radial components and columns. The thermal conductivity could then be calculated for each section, varying the diameter of the strut.

The smallest diameter achievable with our current casting procedure is one millimeter (1mm). It was determined that, even with the smallest diameter strut, the target thermal conductivities could not be achieved. The initial bulk-thermal-conductivity equation derived was based on aluminum as the material of the Cube. New equations were derived by changing the material of the Cube in the FEA. Comparing the derived equations showed that the original equation can be scaled to fit the new equations by multiplying the original with the factor $k_{new\ material}/k_{original}$. This resulted in a maximum of seven percent (7%) error when comparing the calculated bulk thermal conductivity of the original equation and the FEA results of the new material. The target thermal conductivity could then be achieved by using Mold Star 22™, a material with a thermal conductivity of 43.2 W/mK, to cast the one-millimeter-diameter struts.

The preliminary structure was chosen to have 5 columns and 15 radial components (Figures 6,7). The hemi-spherical top part of the structure was not designed based on the derived bulk-thermal-conductivity equation, but was approximated to match the desired conductivities while maintaining good structural connectivity to the lower cylindrical section. A 3-D structure was generated and cast, as was a finned thermal-management device of the same material and total mass for reference (Figure 7). The engineered structure had twice the surface area of the finned component.

Fabrication

The one-millimeter (1 mm) minimum feature size on a structure of this size and complexity is quite a challenge to produce. The weight of the alloys is also of concern. Certainly, direct-metal processes are an option, but were not used due to limitations of time and funding, as well as uncertainty of the thermal properties of the additively-manufactured metal.

The selected method for fabricating the thermal-management structure was to use additive manufacturing to produce a pattern for investment casting. This approach provides the potential for investigating the performance of many alloys and composites. Indeed, while the investigations to date have included exclusively air-filled structures, the principles will be extended to include solid fill. This is of particular interest for combining wear resistance and heat dissipation in the structural design of components.

The patterns for the thermal-management devices were created in nylon at the Milwaukee School of Engineering (MSOE), using Selective Laser Sintering™ (SLS™), and then encased in ceramic. After burning out the nylon, the empty ceramic shell was filled with the molten Moldstar 22™ alloy, using MSOE's proprietary high-resolution investment-casting process.

Results

A. Unit-Lattice Characterization:

The resultant unit-cell thermal resistances and conductivities are tabulated in Appendix C. Multiple relation forms were attempted in the regressions, including: quadratic; second-order cross-multiplied; third order; second-order quadratic; linear cross-multiplied; linear; and, homogeneous second-order [Appendix D]. Comparing the errors of these relations in predicting the performance of the unit cells, it was found that the second-order cross-multiplied form had the lowest error; however, this is not definitive: LINEST is limited to 17 terms; and, efforts were constrained by time.

Effects of Convection

Initial analyses that included the development of internal convective flow returned unexpected results: heat transfer in the orthogonal directions showed negligible change. The majority of the heat was flowing through the solid. This makes sense if thought about as an electrical model. Each Cube can be thought of as three resistances in parallel, solid, fluid and a series combination of solid and fluid [Yu et. al. 2006]. Even if the total resistance of the fluid resistor decreased, e.g. by changing the fluid, the thermal resistivity is still substantially larger than that of the solid metal used. This raised the question of, "What would happen if the conductivity of the solid decreased, thereby increasing its thermal resistance?"

To show the relationship between material and convection, a new model was used, consisting of a block of air, surrounded by a block of metal. By varying the thickness of the metal surrounding the air, a plot of percent difference in heat transfer (between convective and stagnant air) versus solid thickness could be made for various materials. The plot generated shows that as the conductivity of the material increases, or as the amount of solid material around the air increases, the effects of convection becomes less prominent (Figure 5). But, even with a material of low conductivity, such as Inconel, the percent difference between convective and stagnant air is low (0.6% at a 100K delta). The exponential increase in the significance of the internal convection, with decreasing solid volume fraction and conductivity, shows that the solid material must have thermal conductivity close to that of the contained fluid for cellular convective flow to be of significance, relative to the stagnant conductivity.

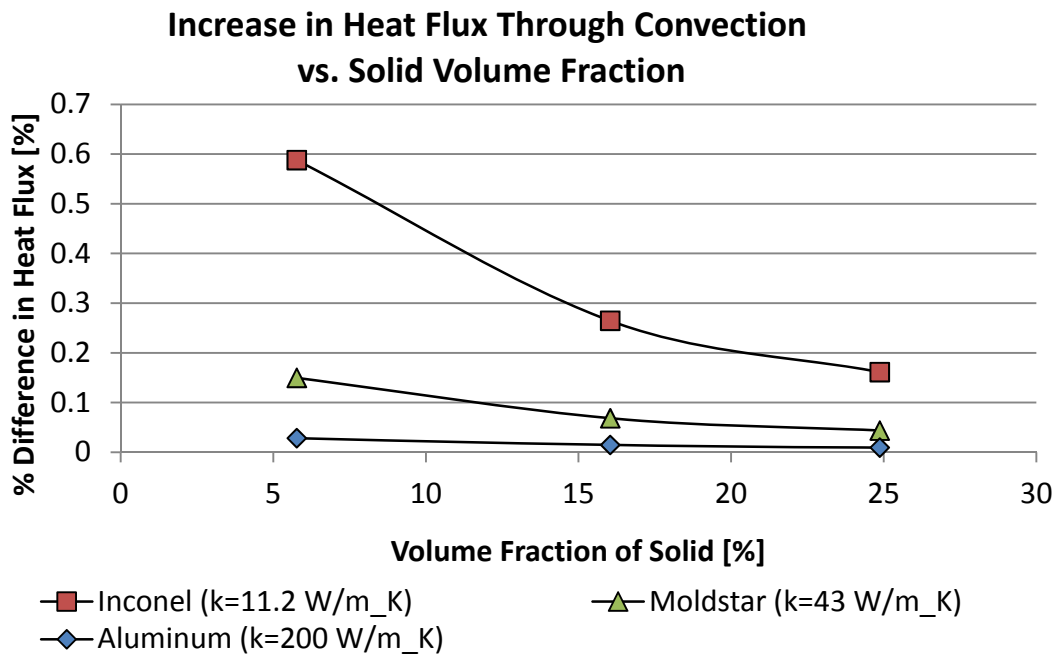


Figure 5: This plot shows the dependence of the heat flow rate through the unit cell on the development of cellular convective flow, at a $\Delta T = 100K$. Even for solid materials of low thermal conductivity, and at low volume fraction, the change in heat flow is less than one percent in comparison to stagnant air. Convective flow through a lattice structure, however, will produce a significant difference in the heat flow rate.

B. Structure:

A Matlab® script was composed to assist in the design of the preliminary thermal-management structure, incorporating the derived geometric relations to maintain “square” unit cells, calculating the resultant outer radius of the structure as a function of the number of angular and radial divisions (Figure 6). For the one-millimeter-minimum-diameter constraint, a large outer radius of 40 mm was selected, corresponding to fifteen angular and five radial divisions. Certainly, with higher-resolution fabrication processes, more compact (smaller radius) designs can be achieved.

Outer Radius vs. Slices and Divisions

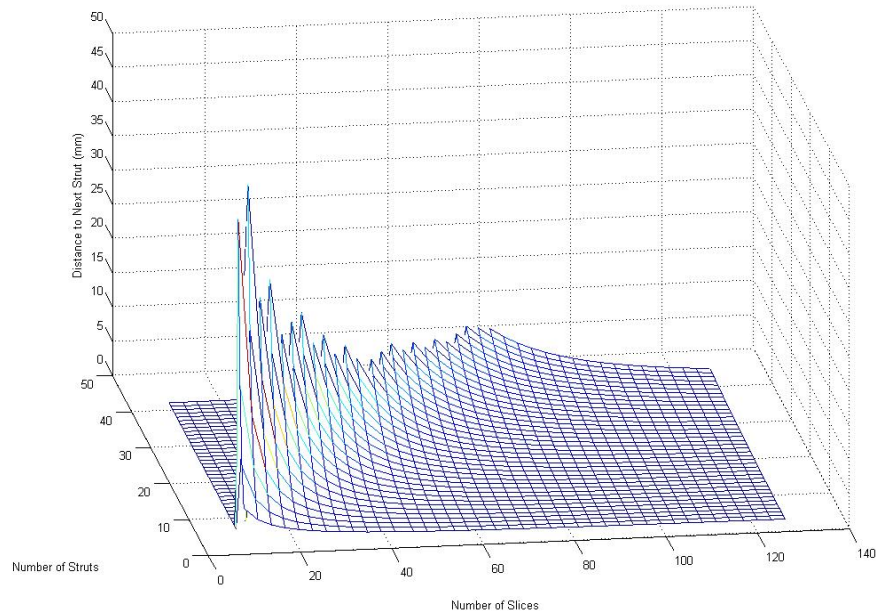


Figure 6: Outer radius of the thermal-management structure (vertical axis [mm]), constrained by “squareness” of the resulting cells. The X-axis represents the number of angular divisions, while the Y-axis represents the number of radial divisions. Choosing 15 slices (angular divisions) and 5 layers (radial divisions), the cell sizes in each layer were determined from the underlying relation.

For the Moldstar 22™ material, this provided effective conductivities across the radial divisions of $k_{\text{effective}} = \{6.4371, 2.5359, 0.9432, 0.3113, 0.0731\}$. With all necessary parameters defined, the model was generated, fabricated and cast, along with a “reference” finned heat sink (Figure 7).

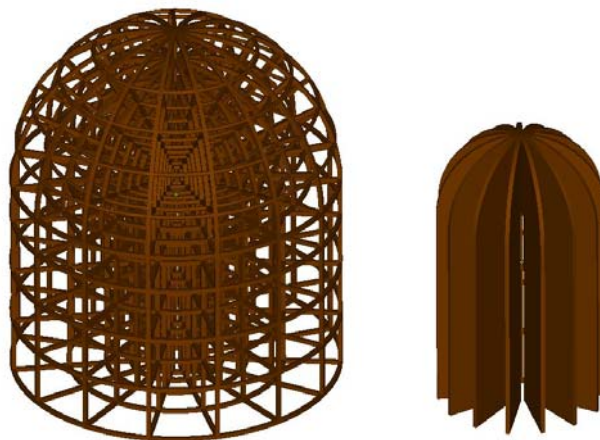


Figure 7: (Left) engineered thermal-management structure, (right) finned heat sink of equal mass and material, but half of the surface area.

C. *Experimental Results*

The engineered structure, finned component, and a cylindrical piece of aluminum foam were tested for their thermal performance in providing a safe contact temperature. A heating element was placed inside each structure. The voltage to the heating element was controlled with a variable supply; and, both voltage and current were measured. A type-K thermocouple was used to record the temperature of the structure. Measurements were taken after five minutes of supplying the measured power to the heating element, for six consecutive power settings. The measured temperatures were then plotted as functions of the input power (Figure 8).

The engineered structure performed exceptionally better than the finned component and aluminum foam. The finned component outperformed the aluminum foam, but both were harmful to touch after the second measurement.

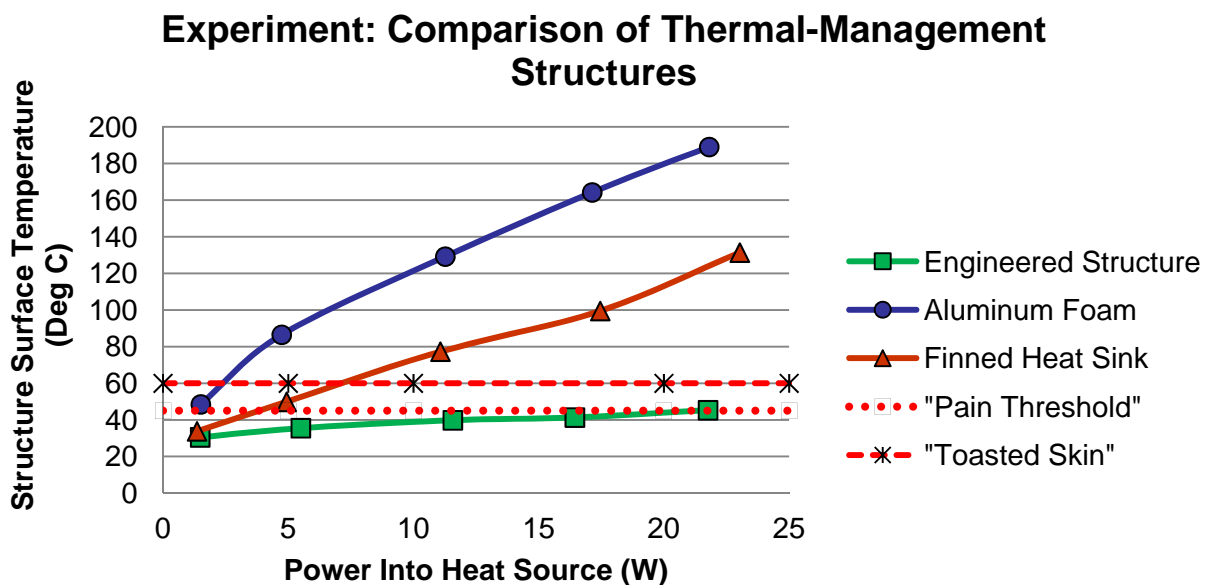


Figure 8: Experimental results of testing the engineered structure, aluminum foam and a finned heat sink. Only the engineered structure provided a safe contact temperature.

It should be noted that the foam structure was not of the same material, nor of the same mass as the engineered structure or finned component: an off-the-shelf cylindrical foam piece was used; but, its size was close to that of the finned structure. The small pore sizes of the aluminum foam, in comparison to the cavities in the engineered structure, also did not allow for any significant fluid flow through the component, or radiation. Fluid flow through the engineered structure, driven by buoyancy, and radiation through the radially-expanding cavities, allowed the structure to maintain a safe contact temperature even past its original design specification.

D. *Varying the Design:*

2-D axi-symmetric FEA models were analyzed, varying the number of columns in the analysis from three to seven. The results show that, with fewer columns, the structure is able to

achieve a greater temperature drop. Even though a structural analysis was not performed on the current design, fabricating a structure with less supports could lead to a fragile component.

The model was also evaluated with Inconel (thermal conductivity approximately 11.2 W/mK). The results showed that, with the current geometry, Inconel could achieve a temperature drop over three times that achieved with Mold Star 22™. This means that using Inconel as the material of the component could lead to more compact, and stronger, components. The rate of heat dissipation will drop, however, increasing the core temperature for a given heat production rate. This balance requires optimization in the design.

Strut diameters smaller than one millimeter were also investigated. For Inconel structures, an engineered TMS with a strut diameter of 0.5 mm had twice the performance of a structure with a strut diameter of 1 mm. Again, Inconel had nearly three times the performance of Mold Star 22™ at strut diameters of 0.5 mm.

Improvements to the current design can easily be made by varying the material of the component. The components can also have increased effectiveness and greater compactness if manufacturing techniques are improved upon.

Next Steps

Of greatest priority is the application of this research to an integrative thermal-management structure for the powered orthosis. The engine is expected to be operational shortly; and, testing on patients is anticipated in the summer of 2012. In addition to protecting the wearer from the excessive temperatures, investigations are already underway to determine the practicality of integrating thermoelectric generators into the structure to power some of the electrical components, thereby improving system efficiency.

For this work, it was assumed that the lower surface temperatures and higher heat-flux rates of the engineered thermal-management structure, due to convective fluid flows through it, further improves the performance of the component; therefore, no effort was made to account for convective through-flow. To achieve precise metrics, and full understanding of the structure's performance, future research will investigate the fundamental dynamics that both drive and resist this through-flow, including:

- Nusselt number – ratio of convective/conductive heat transfer.
- Darcy flow relation to define resistance to convective through-flow.
- Schmidt number – the ratio of momentum diffusivity (viscosity) and mass diffusivity, used to characterize fluid flows in which there are simultaneous momentum and mass-diffusion convection processes.

To expedite the analyses, a slice of the structure is being used, with “symmetry” boundary conditions on the cut faces (Figure 9).

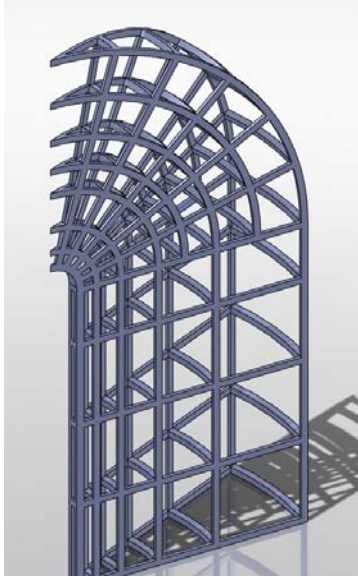


Figure 9: This is a vertical slice of a revolutionary-generated structure that is being used for analyses of the performance of the resultant structure. “Symmetry” boundary conditions are applied to the cut faces to reflect the missing geometry. A similar structure will be fit around the small internal-combustion engine on the powered orthosis to dissipate heat and protect the wearer from prolonged exposure to high temperatures.

Ten geometric configurations of each unit-lattice cell were analyzed, providing a total of 27 data points for each through the assumption of symmetry and negligible influence of fluid convection. As with the structural characterizations done in the past, more configurations could be analyzed for greater resolution or fidelity, particularly in the case of very small solid geometries.

The second-order, cross-multiplied form was selected as the best representation, out of the seven that were considered, of the geometry-dependence of the unit-lattice’s effective thermal conductivity, but is certainly not the only applicable form. Simpler relations may meet the tolerance of the application, and may even be more accurate.

While work has begun to determine the effective thermal conductivity of these unit-lattice structures in directions not aligned with their orthogonal members, further research is required to determine the extent of their effective-conductivity anisotropy. For those cases where internal natural convection can be neglected, the thermal characteristics are expected to be orthotropic, just as their structural properties are, with constant factors that relate to the orthogonal directions, e.g. the fraction of the x-direction conductivity that contributes to the diagonal.

Future efforts will also investigate the potential for automating the optimization of the distribution of effective conductivity throughout the thermal-management structure. This will allow for higher resolution and better performance, while allowing the designer to consider more options as well.

Conclusions

Passive thermal management of components can be achieved through the design of components using engineered lattices. To this end, the geometry-dependent effective bulk thermal conductivities of three unit lattice structures were determined for the three orthogonal directions. The heat flux through the unit cell scaled linearly to its size, resulting in a constant conductivity, simplifying the design of gradient lattice structures.

While internal cellular convection may develop and alter the effective bulk conductivity, the investigations showed that the effects were negligible for the materials under consideration. Generally, the target performance of the thermal-management structure can be attained by varying the base material and geometry.

The engineered thermal-management structure outperformed aluminum foam and an equal-mass finned component in providing a safe contact temperature. Convective flow of air through the final structure, however, did alter the performance significantly. While this improved the safety of the device, it does present a challenge in accurately predicting performance. This is being addressed in current research efforts.

Benefits of this approach to thermal management include the potential for creating integrated, minimal-mass, multifunctional components, and for optimizing temperature gradients for energy recovery through thermoelectric generation. Current limitations are the resolution achievable and the small number of direct-metal alternatives to casting alloys.

Acknowledgements

- This material is based upon work supported by the National Science Foundation's Engineering Research Center, the Center for Compact and Efficient Fluid Power (CCEFP), under Grant No. EEC-0540834. Any opinions, findings, and conclusions or recommendations expressed in this material are those of the author and do not necessarily reflect the views of the National Science Foundation.
- Paul Michael (MSOE Fluid-Power Institute) - pointing out relevance of Rohmax's research and new thermoelectric materials.
- Toni Borel - REU investigation of means for thermoelectric recapture of waste-heat energy.
- Vito Gervasi and assistants (MSOE Rapid-Prototyping Research) - casting of components.
- Sheku Kamara and assistants (MSOE Rapid-Prototyping Center) - fabrication of component patterns.

References

Canter, Neil Ph.D. "Electricity from Automotive Exhaust," Tribology & Lubrication Technology, pp. 10-11, March 2011.

The Center for Compact and Efficient Fluid Power. (n.d.). Fluid Power | Center for Compact & Efficient Fluid Power. Retrieved August 31, 2011, from The Center for Compact and Efficient Fluid Power Web Site: <http://www.ccefp.org/>

Cook, Douglas and Gervasi, Vito. "High-Performance, Multi-Functional, Fluid-Power Components Using Engineered Materials," Proceedings of the 52nd National Conference on Fluid Power. Las Vegas, Nevada (2011).

Cook, Douglas; Knier, Bradley; Gervasi, Vito; and, Stahl, Douglas Ph.D. "Automatic Generation of Strong, Light, Multi-Functional Structures from FEA Output." Proceedings of the 21st Annual International Solid Freeform Fabrication (SFF) Symposium. Austin, Texas (2010).

Davis, Richard A. "An Explicit Expression for the Break-Even Radius of Insulation on a Cylinder in Cross-Flow," Journal of Engineering, Computing and Architecture, Vol. 1, Issue 1 (2007).

Herzog, S. N. and Neveu, C. D. "Relative Impact of Hydromechanical and Volumetric Losses on Hydraulic Pump Efficiency at High and Low Temperatures," Proceedings of the 52nd National Conference on Fluid Power. Las Vegas, Nevada (2011).

Human Assist Devices - Fluid Powered Ankle-Foot Orthosis (Test Bed 6). (n.d.). Fluid Power | Center for Compact & Efficient Fluid Power. Retrieved August 31, 2011, from The Center for Compact and Efficient Fluid Power Web Site: <http://www.ccefp.org/research/test-beds/fluid-powered-ankle-foot-orthosis>

Incropera, F. and Dewitt, D. "Introduction to heat transfer," John Wiley and Sons Inc., New York, NY, United States (1985).

Kim, T.; Zhao, C.Y.; Lu, T.J.; and, Hodson, H.P. "Convective Heat Dissipation with Lattice-Frame Materials," Mechanics of Materials, 36, pp. 767-780 (2004).

Kulkarni, M. R. "Critical Radius for Radial Heat Conduction: A Necessary Criterion But Not Always Sufficient," Applied Thermal Engineering, 24, pp. 967-979 (2004).

Project 2B.2: Miniature HCCI Free-piston Engine Compressor. (n.d.). Fluid Power | Center for Compact & Efficient Fluid Power. Retrieved August 31, 2011, from The Center for Compact and Efficient Fluid Power Web Site: <http://www.ccefp.org/research/thrust-2-compactness/project-2b2>

Schneider, T.; Alley, R.; Koester, D.; and Lee, S. "Thin Film Thermoelectric Power Generation." Nextreme Thermal Solutions. Research Triangle Park, NC (2007).

Seepersad, Carolyn C.; Allen, Janet K.; McDowell, David L.; and, Mistree, Farrokh. "Multifunctional Topology Design of Cellular Material Structures," Proceedings of ASME IDETC/CIE 2006. Paper number DETC2006-99373. Philadelphia, Pennsylvania (2006).

Shorter, K. A. et al. "A Portable-Powered-Ankle-Foot-Orthosis for rehabilitation," Journal of Rehabilitation Research & Development, Accepted 2010.

Straatman, A. G.; Gallego, N. C.; Yu, Q.; Betchen, L.; and, Thompson, B. E. "Forced Convection Heat Transfer and Hydraulic Losses in Graphitic Foam," ASME Journal of Heat Transfer, 129, pp. 1237-1245 (2007).

Tian, L.; Kittelson, D.B.; and, Durfee, W.B. "Experimental Tests and Simulations of A 1.5 cc Miniature Glow-Ignition Two-Stroke Engine", SAE Technical Paper, paper number 2010-32-0018 (2010).

Wadley, Haydn N. G. "Cellular Metals Manufacturing," Advanced Engineering Materials, 4, pp. 726-733 (2002).

Yu, Qijun; Thompson, Brian E.; and, Straatman, Anthony G. "A Unit Cube-Based Model for Heat Transfer and Fluid Flow in Porous Carbon Foam," ASME J. Heat Transfer, 128, pp. 355-360 (2006).

Appendix A

Calculating thermal resistance of the composite Cube unit cell:

$$\frac{1}{R_{x_{total}}} = \frac{t_z (Z - 2t_x)}{\left(\frac{2t_z}{k_{solid}} + \frac{(X - 2t_z)}{k_{fluid}} \right)} + \frac{t_y (Y - 2t_x)}{\left(\frac{2t_y}{k_{solid}} + \frac{(X - 2t_y)}{k_{fluid}} \right)} + \frac{4t_x^2 k_{solid} + (Z - 2t_y)(Y - 2t_z) k_{fluid}}{X}$$

For X=Y=Z = L, tx=ty=tz = t, L-2t = a, 2t = b (equilateral Cube with equiradial struts):

$$\frac{1}{R_{x_{total}}} = \frac{1}{\left(\frac{1}{ak_{solid}} + \frac{1}{bk_{fluid}} \right)} + \frac{b^2 k_{solid} + a^2 k_{fluid}}{L}$$

For C = k_{fluid}/k_{solid} (or, generally, k_{fill}/k_{structure}):

$$\frac{1}{R_{x_{total}}} = k_{solid} \left[\frac{1}{\left(\frac{1}{a} + \frac{1}{bC} \right)} + \frac{b^2 + a^2 C}{L} \right]$$

Appendix B

Comparative effective thermal conductivities of the Cube unit cell (composed of aluminum and filled with stagnant air) using two analytical approaches. Surface integration was used in both approaches to calculate the total heat flow rate.

Bare unit cell:

X	Y	Z	kxx	kyy	kzz
0.2	0.2	0.2	5.424803	5.434173	5.456732
0.2	0.2	0.5	7.544803	7.550079	31.93528
0.2	0.2	0.8	13.64067	13.6439	80.88736
0.2	0.5	0.5	7.818543	36.20425	36.19969
0.2	0.5	0.8	13.68291	50.68433	84.51748
0.2	0.8	0.8	14.23811	95.97161	95.98736
0.5	0.5	0.5	39.04016	39.05496	38.99445
0.5	0.5	0.8	51.17823	51.16154	87.92441
0.5	0.8	0.8	56.13094	98.55417	98.55724
0.8	0.8	0.8	106.2783	106.2817	106.2629

Incorporating adjacent copper blocks:

X	Y	Z	kxx	kyy	kzz
0.2	0.2	0.2	5.246288	5.242205	5.241969
0.2	0.2	0.5	7.250945	7.249685	26.37031
0.2	0.2	0.8	12.76008	12.7637	56.13559
0.2	0.5	0.5	7.785621	35.32829	35.33074
0.2	0.5	0.8	13.66739	50.40666	82.27342
0.2	0.8	0.8	14.2213	95.05875	95.06878
0.5	0.5	0.5	38.5927	38.58547	38.58037
0.5	0.5	0.8	50.92814	50.93768	86.33769
0.5	0.8	0.8	56.06813	98.00734	98.02823
0.8	0.8	0.8	106.3987	106.3745	106.3674

Appendix C

Resultant thermal resistances and conductivities of the composite unit cells (filled with stagnant air):

Simple Cube:

Heat flow rate [W]

X	Y	Z	Q _{xx}	Q _{yy}	Q _{zz}
0.2	0.2	0.2	13.3152	13.3152	13.3146
0.2	0.2	0.5	18.4174	18.4142	66.9806
0.2	0.2	0.8	32.4106	32.4198	142.5844
0.5	0.2	0.5	76.2627	19.0345	76.2672
0.5	0.5	0.5	82.1697	82.1568	82.1477
0.5	0.5	0.8	103.1032	103.1186	153.1742
0.8	0.2	0.5	148.0653	32.4946	102.26
0.8	0.2	0.8	163.6618	33.7241	163.6735
0.8	0.5	0.8	167.0688	111.2306	167.0927
0.8	0.8	0.8	176.4059	176.3797	176.372

Resistance [K/W]

X	Y	Z	R _{xx}	R _{yy}	R _{zz}
0.2	0.2	0.2	0.0047183	0.0047183	0.004718508
0.2	0.2	0.5	0.003376	0.0033766	0.000836204
0.2	0.2	0.8	0.0018636	0.001863	0.000325476
0.5	0.2	0.5	0.000719	0.0032624	0.000718921
0.5	0.5	0.5	0.0006582	0.0006583	0.000658366
0.5	0.5	0.8	0.0004987	0.0004986	0.000294194
0.8	0.2	0.5	0.0003087	0.0018584	0.000503902
0.8	0.2	0.8	0.0002672	0.0017861	0.000267175
0.8	0.5	0.8	0.0002592	0.000453	0.000259109
0.8	0.8	0.8	0.0002387	0.0002388	0.000238795

Conductivity [W/m*K]

X	Y	Z	K _{xx}	K _{yy}	K _{zz}
0.2	0.2	0.2	5.3833067	5.3833067	5.383057596
0.2	0.2	0.5	7.5237151	7.5223587	30.3753531
0.2	0.2	0.8	13.629656	13.633789	78.03958014
0.5	0.2	0.5	35.328289	7.7856209	35.33074161
0.5	0.5	0.5	38.592698	38.58547	38.58037165
0.5	0.5	0.8	50.928138	50.937682	86.33769021
0.8	0.2	0.5	82.273423	13.667395	50.40666437
0.8	0.2	0.8	95.058753	14.2213	95.0687792
0.8	0.5	0.8	98.00734	56.068134	98.02823231
0.8	0.8	0.8	106.3987	106.37449	106.3673755

Ultra Cube:

Heat flow rate [W]

X	Y	Z	Qxx	Qyy	Qzz
0.2	0.2	0.5	99.0977	99.1023	123.4554
0.2	0.2	0.8	178.687	178.685	191.4161
0.5	0.5	0.8	161.8846	161.8754	185.7758
0.8	0.2	0.5	199.8318	197.9088	192.2217
0.8	0.2	0.8	200.2388	211.2022	200.2393
0.8	0.5	0.8	188.6063	201.0755	188.6045
0.5	0.2	0.5	117.2653	148.9309	117.2619

Resistance [K/W]

X	Y	Z	Rxx	Ryy	Rzz
0.2	0.2	0.5	0.000524	0.000524	0.000396
0.2	0.2	0.8	0.000234	0.000234	0.00021
0.5	0.5	0.8	0.000272	0.000272	0.00022
0.8	0.2	0.5	0.000196	0.000199	0.000209
0.8	0.2	0.8	0.000195	0.000178	0.000195
0.8	0.5	0.8	0.000215	0.000194	0.000215
0.5	0.2	0.5	0.000423	0.000306	0.000423

Conductivity [W/m*K]

X	Y	Z	Kxx	Kyy	Kzz
0.2	0.2	0.2	5.383307	5.383307	5.383058
0.2	0.2	0.5	48.47011	48.47291	64.20862
0.2	0.2	0.8	108.5211	108.5192	120.926
0.5	0.5	0.8	50.92814	50.93768	86.33769
0.5	0.5	0.8	93.54371	93.53591	115.3084
0.8	0.2	0.5	129.6901	127.6455	121.7447
0.8	0.2	0.8	130.1261	142.3206	130.1266
0.8	0.5	0.8	118.1027	131.026	118.1009
0.5	0.2	0.5	60.02298	82.95389	60.02071
0.8	0.8	0.8	106.3987	106.3745	106.3674

Super Cube:

Heat flow rate [W]

X	Y	Z	Qxx	Qyy	Qzz
0.2	0.2	0.2	13.3167	13.3152	13.3146
0.2	0.2	0.5	104.7102	101.1266	110.8746
0.2	0.2	0.8	200.2422	199.3812	198.9372
0.2	0.5	0.5	108.9378	129.7484	129.7721
0.2	0.5	0.8	203.0444	206.6968	204.0729
0.2	0.8	0.8	206.4395	211.3989	211.4009
0.5	0.5	0.5	82.1697	82.1568	82.1474
0.5	0.5	0.8	193.607	193.4543	194.1705
0.5	0.8	0.8	200.5455	208.0136	208.0219
0.8	0.8	0.8	176.4059	176.3797	176.372

Resistance [K/W]

X	Y	Z	Rxx	Ryy	Rzz
0.2	0.2	0.2	0.004718	0.004718	0.004719
0.2	0.2	0.5	0.000489	0.000511	0.000455
0.2	0.2	0.8	0.000195	0.000197	0.000197
0.2	0.5	0.5	0.000465	0.00037	0.00037
0.2	0.5	0.8	0.000191	0.000185	0.000189
0.2	0.8	0.8	0.000186	0.000178	0.000178
0.5	0.5	0.5	0.000658	0.000658	0.000658
0.5	0.5	0.8	0.000206	0.000206	0.000205
0.5	0.8	0.8	0.000195	0.000183	0.000183
0.8	0.8	0.8	0.000239	0.000239	0.000239

Conductivity [W/m*K]

X	Y	Z	Kxx	Kyy	Kzz
0.2	0.2	0.2	5.383929	5.383307	5.383058
0.2	0.2	0.5	51.92802	49.70912	55.83858
0.2	0.2	0.8	130.1297	129.2087	128.7358
0.2	0.5	0.5	54.5969	68.60428	68.62111
0.2	0.5	0.8	133.1633	137.2019	134.2907
0.2	0.8	0.8	136.9142	142.5476	142.5499
0.5	0.5	0.5	38.5927	38.58547	38.58037
0.5	0.5	0.8	123.1624	123.0055	123.7427
0.5	0.8	0.8	130.4554	138.682	138.6914
0.8	0.8	0.8	106.3987	106.3745	106.3674

Appendix D

Regression formats used. The Y-intercept was assumed zero due to the comparatively low thermal resistance of air.

Linear:

$$K(x, y, z) = A\phi x + B\phi y + C\phi z$$

Linear Cross-Multiplied:

$$K(x, y, z) = A\phi x\phi y\phi z + B\phi x\phi y + C\phi x\phi z + D\phi y\phi z + E\phi x + F\phi y + G\phi z$$

Second-Order Quadratic:

$$K(x, y, z) = A\phi x^2 + B\phi y^2 + C\phi z^2$$

Quadratic:

$$K(x, y, z) = A\phi x^2 + B\phi y^2 + C\phi z^2 + D\phi x + E\phi y + F\phi z$$

Homogeneous Second-Order:

$$K(x, y, z) = A\phi x^2 + B\phi y^2 + C\phi z^2 + D\phi x\phi y + E\phi x\phi z + F\phi y\phi z$$

Second-Order Cross-Multiplied:

$$K(x, y, z) = A\phi x^2 + B\phi y^2 + C\phi z^2 + D\phi x\phi y + E\phi x\phi z + F\phi y\phi z + G\phi x + H\phi y + I\phi z$$

Third Order:

$$K(x, y, z) = A\phi x^3 + B\phi y^3 + C\phi z^3 + D\phi x^2 + E\phi y^2 + F\phi z^2 + G\phi x + H\phi y + I\phi z$$

Appendix E

Resultant homogeneous second-order relations for the effective thermal conductivities of the three different unit cell types. Again, the Y-intercept was assumed zero due to the comparatively low thermal resistance of air.

Simple Cube:

$$K_{xx}(x, y, z) = 77.287\phi x^2 + 36.415\phi y^2 + 36.360\phi z^2 + 28.374\phi x\phi y + 28.3424\phi x\phi z - 24.271\phi y\phi z + 28.345\phi x - 20.039\phi y - 19.98\phi z$$

$$K_{yy}(x, y, z) = 36.367\phi x^2 + 77.293\phi y^2 + 35.421\phi z^2 + 28.328\phi x\phi y - 24.285\phi x\phi z + 28.360\phi y\phi z - 19.977\phi x + 28.348\phi y - 20.036\phi z$$

$$K_{zz}(x, y, z) = 36.425\phi x^2 + 36.371\phi y^2 + 77.297\phi z^2 - 24.290\phi x\phi y + 28.354\phi x\phi z + 28.323\phi y\phi z - 20.036\phi x - 19.977\phi y + 28.348\phi z$$

Ultra Cube:

$$K_{xx}(x, y, z) = 232.045\phi x^2 + 176.688\phi y^2 + 176.715\phi z^2 - 205.445\phi x\phi y - 205.443\phi x\phi z - 120.530\phi y\phi z + 26.423\phi x + 37.803\phi y + 37.777\phi z$$

$$K_{yy}(x, y, z) = 176.721\phi x^2 + 232.051\phi y^2 + 176.694\phi z^2 - 205.458\phi x\phi y - 120.544\phi x\phi z - 205.460\phi y\phi z + 37.779\phi x + 26.426\phi y + 37.806\phi z$$

$$K_{zz}(x, y, z) = 176.698\phi x^2 + 176.725\phi y^2 + 232.055\phi z^2 - 120.549\phi x\phi y - 205.465\phi x\phi z - 205.463\phi y\phi z + 37.806\phi x + 37.779\phi y + 26.426\phi z$$

Super Cube:

$$K_{xx}(x, y, z) = 198.534\phi x^2 + 232.108\phi y^2 + 228.276\phi z^2 - 183.180\phi x\phi y - 186.927\phi x\phi z - 206.625\phi y\phi z + 50.697\phi x + 19.039\phi y + 25.532\phi z$$

$$K_{yy}(x, y, z) = 228.283\phi x^2 + 198.54\phi y^2 + 232.115\phi z^2 - 186.941\phi x\phi y - 206.639\phi x\phi z - 183.194\phi y\phi z + 25.534\phi x + 50.699\phi y + 19.041\phi z$$

$$K_{zz}(x, y, z) = 232.119 + 228.287\phi y^2 + 198.544\phi z^2 - 206.644\phi x\phi y - 183.199\phi x\phi z - 186.947\phi y\phi z + 19.041\phi x + 25.534\phi y + 50.699\phi z$$